COMMUNICATIONS IN COMPUTATIONAL PHYSICS
Vol. **2**, No. 6, pp. 1125-1138

Commun. Comput. Phys.
December 2007

Lattice Boltzmann Method for Simulating the Temperature Jump and Velocity Slip in Microchannels

Lin Zheng[1,*], Bao-Chang Shi[1,2] and Zhen-Hua Chai[2]

[1] *Department of Mathematics, Huazhong University of Science and Technology, Wuhan 430074, China.*
[2] *State Key Laboratory of Coal Combustion, Huazhong University of Science and Technology, Wuhan 430074, China.*

Received 1 November 2006; Accepted (in revised version) 19 December 2006

Communicated by Dietrich Stauffer

Available online 15 June 2007

Abstract. The velocity slip and temperature jump in micro-Couette flow are investigated with the lattice Boltzmann method (LBM). A new slip boundary condition with the non-equilibrium extrapolation scheme is used in a thermal lattice Boltzmann model (TLBM) where double distribution functions are used to simulate the velocity and the temperature fields in order to capture the velocity slip and the temperature jump of the wall boundary. The simulated velocity and temperature profiles are in good agreement with the analytic results, which shows the suitability of the present model and the new boundary treatment for describing thermal microflows with viscous heat dissipation.

PACS: 05.10.-a, 47.11-j, 47.61.-k

Key words: Lattice Boltzmann, velocity slip, temperature jump.

1 Introduction

With the rapid development in Micro-electro-mechanical systems (MEMS), flow and heat transfer in micro devices have become an area that receives a significant attention over the last decade [1–3]. The mechanism of the microscopic flow and heat transfer is quite different from that of macroscopic counterparts because the characteristic length of the flow H is of comparable order of magnitude to the mean free path λ, and the inter-molecular interactions are manifested. The microscopic flows are usually characterized by a dimensionless parameter – the Knudsen number $Kn = \lambda/H$. Theoretically, when $Kn > 0.01$,

*Corresponding author. *Email addresses:* zhlinhust@163.com (L. Zheng), sbchust@yahoo.com (B. C. Shi), ishustczh@126.com (Z. H. Chai)

traditional hydrodynamic descriptions such as the Navier-Stokes equations (NSE) and the Fourier heat conduction equation are invalid and the solvers of the full Boltzmann equation [4, 5], the particle-based methods such as molecular dynamics [6], and the direct simulation Monte Carlo (DSMC) [7] are often used for numerical studies. However, the computational effort of this traditional methods suffers from the expensive computational cost and high statistical noise in simulating low-speed flows. Fortunately, the velocity slip and temperature jump in the microflow still could be captured in the slip-flow regime by NSE with proper slip boundary conditions.

Recently, the LBM has been considered as an efficient numerical tool for simulating fluid flows and transport phenomena based on kinetic equations and statistical physics. Because of its distinctive advantages over conventional numerical methods, the LBM has become an attractive method for micro-fluidic flows. Some numerical methods based on the gas kinetic theory have been proposed to study the gas flows at finite Knudsen numbers [8-15]. Nie et al. [8] used the halfway bounce-back rule for the slip velocity at the solid surface, but it was considered as a no-slip boundary condition by Succi [9] who introduced the specular bounce-back rule. In the same year, both the specular bounce-back rule and the extrapolation scheme were employed to generate the slip effect by Lim et al. [10]. It was concluded that the LBM is an efficient approach for simulation of microflow. Sofonea and Sekerka [13] studied the effect of various boundary conditions for two dimensional first-order upwind finite difference LBM in the microchannel. It is noticed that all the above works discuss mainly the isothermal microflows, while Sofonea and Sekerka [14] and Shu et al. [15] focused on the implementation of diffusion reflection boundary conditions for the TLBM. Two series relaxation time expressions are compared with the analytical velocity and temperature profile in [14]. However, an extra factor (1.15 is chosen in part VI in Ref. [14]) has to be added to obtain a better capture of the slip velocity. Shu et al. [15] analyze the kinetic boundary condition and get similar boundary conditions as that of Karniadakis and Beskok [3]. However, they ignore the viscous dissipation in their analysis. Moreover, for more complex geometry, the above boundary conditions may not be trivial. In Tian et al. [16], they use the classical Maxwell first-order slip boundary conditions. However, they have to deal with the viscous dissipation term in the simulation with complex space discretization. Therefore, one of the key points in the micro-fluidic system is about the appropriate slip boundary conditions in the LBM.

The purpose of present study is to propose a new slip boundary condition using the non-equilibrium extrapolation scheme proposed by Guo et al. [17] for LBM. For convenience, our discussion will refer to a recently introduced TLBM in two dimensions [18], which will be briefly reviewed in Section 2. The new slip boundary conditions and the relaxation time, as well as the definition of the mean free path and the Knudsen number, will be addressed in Section 3. Implementation of the non-equilibrium extrapolation scheme for the TLBM is described in Section 4. To test our new slip boundary conditions, two physical problems will be considered. The first one is the problem of heat transport between two parallel walls with the same constant temperatures in the micro-Couette flow. The second one is the micro-Couette flow between two parallel walls with different

temperatures. For these simple problems, analytical solutions based on the continuum models for the temperature and velocity fields are derived in Section 5 and TLBM simulation results are shown in Section 6. The results show that both physical phenomena (velocity slip and temperature jump) are well captured using the new slip boundary conditions.

2 The thermal lattice Boltzmann model

The TLBM [18] can be derived from the discrete Boltzmann equation with the well-known Bhatnagar-Gross-Krook [BGK] collision term [19] using an appropriate procedure for the discretization of the velocity space. The discretization procedure used in [18] involves a set of 9 velocities $\{c_i|i=0,\cdots,8\}$,

$$c_i=\begin{cases}(0,0), & i=0,\\ (\cos[(i-1)\pi/2],\sin[(i-1)\pi/2])c, & i=1,\cdots,4,\\ (\cos[(2i-9)\pi/4],\sin[(2i-9)\pi/4])\sqrt{2}c, & i=5,\cdots,8,\end{cases}$$

where $c=\Delta x/\Delta t$, with the corresponding density distribution functions $f_i=f_i(r,t)$, $(i=0,\cdots,8)$ and the energy distribution function $g_k=g_k(r,t)$, $(k=0,\cdots,4)$. The density distribution function and the energy distribution function satisfy the following equations, respectively:

$$f_i(x+\Delta x,t+\Delta t)-f_i(x,t)=-\frac{1}{\tau}\left(f_i(x,t)-f_i^{(eq)}(x,t)\right)+\Delta t F_i(x,t), \tag{2.1}$$

$$g_k(x+\Delta x,t+\Delta t)-g_k(x,t)=-\frac{1}{\tau_T}\left(g_k(x,t)-g_k^{(eq)}(x,t)\right)+\Delta t R_k(x,t), \tag{2.2}$$

where τ and τ_T are the dimensionless relaxation times, $F_i(x,t)$ and $R_k(x,t)$ are external force term and the source term, respectively. In order to get the viscous dissipation term in the energy equation, we only require that

$$\sum_k R_k=\Phi, \qquad \sum_k c_k R_k=\mathcal{O}(\Delta t),$$

where

$$\Phi=\nu(\nabla\mathbf{u}+\mathbf{u}\nabla):\nabla\mathbf{u}-\frac{2}{3}(\nabla\cdot\mathbf{u})^2,$$

(ν is the kinetic viscosity). When the flow is incompressible, the Φ can be simplified to $\nu(\nabla\mathbf{u}+\mathbf{u}\nabla):\nabla\mathbf{u}$. For simplicity, we set $R_k(x,t)=\frac{1}{5}\Phi$, and the corresponding NSE is easily recovered through the Chapman-Enskog expansion.

The density equilibrium distribution function $f_i^{(eq)}(x,t)$ is given by

$$f_i^{(eq)}=\begin{cases}-\frac{5}{3}P/c^2+s_0(\mathbf{u}), & i=0,\\ \frac{1}{3}P/c^2+s_i(\mathbf{u}), & i=1,\cdots,4,\\ \frac{1}{12}P/c^2+s_i(\mathbf{u}), & i=5,\cdots,8,\end{cases} \tag{2.3}$$

where

$$s_i(\mathbf{u})=\omega_i[3(c_i\cdot\mathbf{u})/c^2+9(c_i\cdot\mathbf{u})^2/(2c^4)-3|\mathbf{u}|^2/(2c^2)],$$

with the weight factor $\omega_0=4/9$, $\omega_{1-4}=1/9$, and $\omega_{5-8}=1/36$.

Following Guo et al. [17,18], the energy density equilibrium distribution function can also be written as

$$g_k^{(eq)}=\frac{T}{5}\left[1+2.5\frac{(c_k\cdot\mathbf{u})}{c^2}\right],\quad k=0,\cdots,4. \tag{2.4}$$

Moreover, the macroscopic pressure P, velocity $\mathbf{u}$, internal energy per unit mass θ, kinematic viscosity ν, and thermal diffusion α are obtained from the following equations

$$P=\frac{3c^2}{5}\left[\sum_{i\neq 0}f_i+s_0(\mathbf{u})\right],\quad \mathbf{u}=\sum_i c_i f_i,\quad \theta=\sum_k g_k, \tag{2.5}$$

$$\nu=\frac{c^2}{3}\Delta t\left(\tau-\frac{1}{2}\right),\quad \alpha=\frac{2c^2}{5}\Delta t\left(\tau_T-\frac{1}{2}\right), \tag{2.6}$$

and the corresponding value of the Prandtl number is $Pr=\nu/\alpha$.

3 A new slip boundary condition

In the slip-flow region, the NSE are solved subject to the velocity slip conditions given by

$$U_{fluid}-U_{wall}=\frac{2-\sigma_v}{\sigma_v}\lambda\frac{\partial U}{\partial y}\Big|_{wall}, \tag{3.1}$$

where σ_v is the tangential momentum accommodation coefficient which depends on the fluid, the solid and the surface finishing, and is determined experimentally to be between 0.2 and 0.8 [21].

If the temperature creep is also considered, the complete slip-flow and temperature jump boundary conditions read as

$$U_{fluid}-U_{wall}=\frac{2-\sigma_v}{\sigma_v}\lambda\frac{\partial U}{\partial y}\Big|_{wall}+\frac{3}{4}\frac{\mu}{\rho T_{gas}}\frac{\partial T}{\partial y}\Big|_{wall}, \tag{3.2}$$

$$T_{fluid}-T_{wall}=\frac{2-\sigma_T}{\sigma_T}\left(\frac{2\gamma}{\gamma+1}\right)\frac{\lambda}{Pr}\frac{\partial T}{\partial y}\Big|_{wall}, \tag{3.3}$$

where μ is the fluid viscosity, γ the specific heat ratio, and σ_T the tangential energy accommodation coefficient.

The above boundary conditions are of first order in Kn. Using an approximate analysis of the motion of the gas in thermal conditions, Beskok and Karniadakin [22] derived

a higher-order slip velocity condition of the form

$$U_{fluid}-U_{wall}=\frac{2-\sigma_v}{\sigma_v}\left[\lambda\frac{\partial U}{\partial y}\Big|_{wall}+\frac{\lambda^2}{2!}\frac{\partial^2 U}{\partial y^2}\Big|_{wall}+\frac{\lambda^3}{3!}\frac{\partial^3 U}{\partial y^3}\Big|_{wall}+\cdots\right], \tag{3.4}$$

$$T_{fluid}-T_{wall}=\frac{2-\sigma_T}{\sigma_T}\left(\frac{2\gamma}{\gamma+1}\right)\frac{1}{Pr}\left[\lambda\frac{\partial T}{\partial y}\Big|_{wall}+\frac{\lambda^2}{2!}\frac{\partial^2 T}{\partial y^2}\Big|_{wall}+\frac{\lambda^3}{3!}\frac{\partial^3 T}{\partial y^3}\Big|_{wall}+\cdots\right]. \tag{3.5}$$

It is known that the second and higher-order derivatives of velocities and temperatures cannot be computed accurately near the wall. By assuming the transition from no-slip flow to slip flow happens smoothly, Beskok [23] proposed the following alternative higher-order boundary condition for the tangential velocity

$$U_{fluid}-U_{wall}=\frac{2-\sigma_v}{\sigma_v}\frac{Kn}{1-bKn}\frac{\partial U}{\partial \overline{y}}\Big|_{wall}, \tag{3.6}$$

$$Kn=\frac{\lambda}{H}, \tag{3.7}$$

where $\overline{y}$ is a non-dimensional variable normalized by H; H is the length scale and b is a higher-order slip coefficient determined from the presumably known no-slip solution,

$$b=\frac{U_0^{''}}{2U_0^{'}}\Big|_{wall}. \tag{3.8}$$

The case with $b=0$ corresponds to the classical Maxwell first-order slip boundary condition. In order to avoid the difficulty of calculating the second-order derivatives of velocities in [23], b is set to be –1 by comparing the velocity scaling with the linearized Boltzmann solution. In general, this higher-order slip coefficient b is an empirical parameter to be determined either experimentally or evaluated from DSMC data. Of course, for more complex geometry, the determination of b may not be trivial. For the purpose of developing a new second-order slip boundary model clarified by Dai et al. [24], the two-dimensional steady compressible momentum and energy equations are considered:

$$\rho\left(u\frac{\partial u}{\partial x}+v\frac{\partial u}{\partial y}\right)=-\frac{\partial P}{\partial x}+\mu\left[\frac{\partial^2 u}{\partial x^2}+\frac{\partial^2 u}{\partial y^2}+\frac{1}{3}\left(\frac{\partial^2 u}{\partial x^2}+\frac{\partial^2 v}{\partial x\partial y}\right)\right], \tag{3.9}$$

$$\rho\left(u\frac{\partial v}{\partial x}+v\frac{\partial v}{\partial y}\right)=-\frac{\partial P}{\partial y}+\mu\left[\frac{\partial^2 v}{\partial x^2}+\frac{\partial^2 v}{\partial y^2}+\frac{1}{3}\left(\frac{\partial^2 v}{\partial x^2}+\frac{\partial^2 u}{\partial x\partial y}\right)\right], \tag{3.10}$$

$$\rho c_p\left(u\frac{\partial T}{\partial x}+v\frac{\partial T}{\partial y}\right)=\kappa\left(\frac{\partial^2 T}{\partial x^2}+\frac{\partial^2 T}{\partial y^2}\right)+2\mu\left[(\frac{\partial u}{\partial x})^2+\left(\frac{\partial v}{\partial y}\right)^2\right]+\mu\left(\frac{\partial v}{\partial x}+\frac{\partial u}{\partial y}\right)^2. \tag{3.11}$$

The above equations can be normalized by the characteristic velocity (u_0); the characteristic length (H); and the characteristic density (ρ_0) and pressure (P_0). Thus, the x-

momentum equation can be rewritten in non-dimensional form as

$$\overline{\rho}\left(\overline{u}\frac{\partial\overline{u}}{\partial\overline{x}}+\overline{v}\frac{\partial\overline{u}}{\partial\overline{y}}\right)=-E\frac{\partial\overline{P}}{\partial\overline{x}}+\frac{1}{Re}\left[\frac{\partial^2\overline{u}}{\partial\overline{x}^2}+\frac{\partial^2\overline{u}}{\partial\overline{y}^2}+\frac{1}{3}\left(\frac{\partial^2\overline{u}}{\partial\overline{x}^2}+\frac{\partial^2\overline{v}}{\partial\overline{x}\partial\overline{y}}\right)\right], \tag{3.12}$$

$$\overline{\rho}\left(\overline{u}\frac{\partial\overline{T}}{\partial\overline{x}}+\overline{v}\frac{\partial\overline{T}}{\partial\overline{y}}\right)=\frac{1}{PrRe}\left(\frac{\partial^2\overline{T}}{\partial\overline{x}^2}+\frac{\partial^2\overline{T}}{\partial\overline{y}^2}\right)+\frac{2Ec}{Re}\left[\left(\frac{\partial\overline{u}}{\partial\overline{x}}\right)^2+\left(\frac{\partial\overline{v}}{\partial\overline{y}}\right)^2\right]+\frac{Ec}{Re}\left(\frac{\partial\overline{v}}{\partial\overline{x}}+\frac{\partial\overline{u}}{\partial\overline{y}}\right)^2, \tag{3.13}$$

where $Re=\rho_0u_0H/\mu$ is the Reynolds number and $E=P_0/(\rho_0u_0^2)$ is the Euler number, $Pr=c_p\mu/\kappa$ is the Prandtl number, $Ec=u_0^2/(c_p\Delta T)$ is the Ec number.

Based on the fact that the vertical velocity component ($\overline{v}$) can be neglected, the x-momentum equation and energy equation can be expressed as

$$\frac{\partial^2\overline{u}}{\partial\overline{y}^2}=Re\frac{\partial\overline{P}}{\partial\overline{x}},\qquad \frac{\partial^2\overline{T}}{\partial\overline{y}^2}=-EcPr\left(\frac{\partial\overline{u}}{\partial\overline{y}}\right)^2. \tag{3.14}$$

Substituting the above relation into equation (2.4) and (2.5), we obtain the second-order slip velocity model:

$$U_{fluid}-U_{wall}=\frac{2-\sigma_v}{\sigma_v}\left[Kn\frac{\partial\overline{U}}{\partial\overline{y}}\Big|_{wall}+\frac{Kn^2}{2}\left(Re\frac{\partial\overline{P}}{\partial\overline{x}}\right)\Big|_{wall}\right], \tag{3.15}$$

$$T_{fluid}-T_{wall}=\frac{2-\sigma_T}{\sigma_T}\left(\frac{2\gamma}{\gamma+1}\right)\frac{1}{Pr}\left[Kn\frac{\partial\overline{T}}{\partial\overline{y}}\Big|_{wall}-\frac{Kn^2}{2}EcPr\left(\frac{\partial\overline{u}}{\partial\overline{y}}\right)^2\Big|_{wall}\right]. \tag{3.16}$$

In this new model, the difficulty of calculating the second-order derivatives of velocities and temperatures are avoided.

Finally, considering the effect of the boundary on the mean-free-path [28] and using present new slip boundary conditions, we can easily relate the Knudsen number to the relaxation time in the lattice Boltzmann evolution equation by the following expression:

$$\tau=\frac{MKn\psi(Kn)}{\sqrt{\pi T/2}}+\frac{1}{2}, \tag{3.17}$$

where M is the characteristic lattice number and $\psi(Kn)=\frac{2}{\pi}\text{atan}(\sqrt{2}Kn^{-3/4})$.

4 Non-equilibrium extrapolation scheme

The hydrodynamic boundary conditions for the lattice Boltzmann method have been studied extensively. In the present model, we can find that the non-equilibrium extrapolation scheme boundary conditions proposed by Guo et al. [17] is particularly useful and can be easily extended to impose the microthermodynamic boundary conditions.

But the non-equilibrium extrapolation scheme boundary conditions should be accomplished with the accuracy of the LBM and the first order non-equilibrium extrapolation scheme is not accurate when simulating the micro-flows. When we simulate the micro-Couette flow, the periodic boundary conditions are applied in the streamwise x direction by treating nodes on the inflow and outflow faces same as the nearest neighbors. For the hot and cool wall, the second order non-equilibrium extrapolation scheme with the new slip boundary conditions is used. The exact form of the method in [17] is as follows: Let x_b be the boundary node, and x_f, x_{ff} be the nearest nodes to the boundary node x_b. First, the boundary node distribution function is separated into the equilibrium part and the non-equilibrium part:

$$f_i(x_b,t)=f_i^{(eq)}(x_b,t)+f_i^{(neq)}(x_b,t). \tag{4.1}$$

For the velocity and temperature boundary conditions, $u_{wall}(x_b,t)$, $T_{wall}(x_b,t)$ at x_b are known while $u(x_b,t)$, $p(x_b,t)$ and $T(x_b,t)$ are unknown. To handle this, we first use $p(x_f,t)$ instead of $p(x_b,t)$, together with (3.15)-(3.16), to obtain $u(x_b,t)$, $T(x_b,t)$ at x_b. Then the equilibrium part at the boundary node x_b can be approximated as

$$\tilde{f}_i^{(eq)}(x_b,t)=f_i^{(eq)}(p(x_f,t),u(x_b,t),T(x_b,t)). \tag{4.2}$$

The non-equilibrium part is approximated by combining the non-equilibrium part of those at x_f and x_{ff} nodes:

$$f_i^{(neq)}(x_b,t)=2(f_i(x_f,t)-f_i^{(eq)}(x_f,t))-(f_i(x_{ff},t)-f_i^{(eq)}(x_{ff},t)). \tag{4.3}$$

Finally, we can get the distribution function at the boundary node x_b as

$$f_i(x_b,t)=\tilde{f}_i^{(eq)}(x_b,t)+f_i^{(neq)}(x_b,t). \tag{4.4}$$

5 Couette flow in microchannels: Temperature jump and velocity slip

In order to have some basis for comparison of our simulations, we first derive the analytic solution of the NSE with this new boundary conditions. We consider a fluid confined between two infinite walls located at $y=0,1$, respectively, which are parallel to the x axis. The upper plate at $y=1$ moves at a constant velocity $u_{WU}=0.1c$, while the bottom plate is at rest. Their temperatures are maintained at θ_{WU} and θ_{WD}, respectively, and the average temperature is

$$T=0.5(\theta_{WU}+\theta_{WD}).$$

We assume that the density and temperature variations across the channel are small enough so that the value of the Knudsen number to be regarded as constant and the vertical velocity is zero everywhere. In this case, the dimensionless density, temperature, and velocity fields depend only on the y coordinate.

With the new slip boundary conditions, by solving the NSE, we obtain the following velocity profile and the temperature jump profile with viscous heat dissipation:

$$u(y)=Ay+B, \tag{5.1}$$

$$\theta(y)=Cy^2+Dy+E, \tag{5.2}$$

with

$$A=\frac{u_{WU}}{1+2hKn},\quad B=\frac{hKnu_{WU}}{1+2hKn},\quad C=-\frac{PrA^2}{2}, \tag{5.3}$$

$$D=-C+\frac{\theta_{WU}-\theta_{WD}+hKn^2PrA^2}{(1+2h_1Kn)}, \tag{5.4}$$

$$E=\theta_{WD}+h_1\left(KnD+Kn^2\frac{PrA^2}{2}\right), \tag{5.5}$$

$$h=\frac{2-\sigma_v}{\sigma_v},\quad h_1=\frac{2-\sigma_T}{\sigma_T}\frac{2\gamma}{\gamma+1}\frac{1}{Pr}. \tag{5.6}$$

6 Simulation results

To test present new slip boundary conditions and compare the TLBM simulation results with the analytical results, namely, (5.1), we further restrict ourselves to two particular cases. The first one is the micro-Couette flow with a constant wall temperature boundary condition. In this case, we have

$$\theta_{WU}=\theta_{WD}=\theta_{wall}=1.0.$$

The second problem we consider here is the thermal Couette flow with different wall temperatures, and temperature difference between the wall is determined by the specified Ec number.

In present work, the TLBM simulations were done to investigate the effect of the new slip boundary conditions. In our simulation, the initial fluid velocity is zero and the temperature is equal to the wall temperature θ_{wall} and the lattice used is a 40×40 square mesh with periodic boundary conditions along the x direction. All results presented in the following have been tested by grid-independent study.

6.1 Thermal micro-Couette flow with constant wall temperature

The velocity slip and temperature jump can be seen in Figs. 1 and 2, which show variations of the dimensionless slip length $\xi=(U_{wall}-U_0)/\gamma$ ($\gamma=\partial u/\partial y$) and the temperature jump $l=(\theta_{wall}-\theta_0)/\dot{\theta}$ ($\dot{\theta}=\partial\theta/\partial y$) with the Knudsen numbers in the range of 0.001 to 0.1. The results obtained by the DSMC, MD and the Maxwell theoretical analysis are also included for comparison. The Maxwell theory predicts that the slip length and temperature jump are about $\xi=1.15Kn$ and $l=0.1333Kn$ [25,27]. As shown in Figs. 1 and 2, the

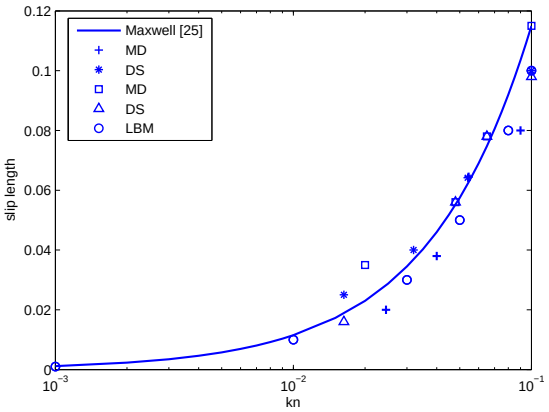

Figure 1: Comparison of [25] and the Maxwell results on the velocity slip length, with $Pr=10$.

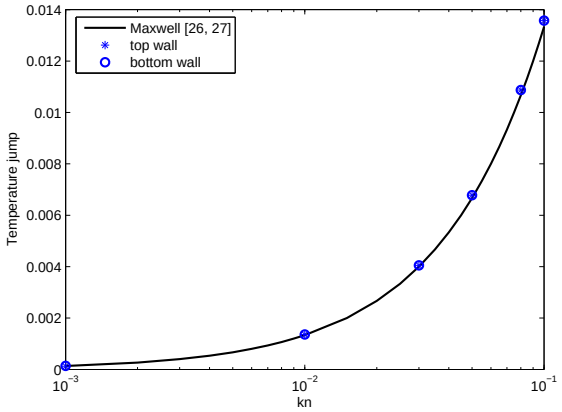

Figure 2: Comparison of [26] and [27] on the temperature jump, with $Pr=10$.

present results are in good agreement with those results, the DSMC approach and MD method [26, 27] in the slip flow regime ($Kn \leq 0.1$). As Kn increases, the present results lie in between the results of the Maxwell theory and those of the DSMC and MD simulations. We also find that the velocity slip and temperature jump increase at the boundary as the Kn increases.

The Knudsen effects on the viscous heat dissipation behaviors can be observed in Figs. 3 and 4. It shows the linear velocity profile and the parabolic temperature profiles, respectively, well established with the Kn varying from 0.001 to 0.1. The four curves represent Kn=0.001, 0.01, 0.05 and 0.1 respectively. The solid lines are analytical solutions and the scatter points are the numerical results.

6.2 Thermal micro-Couette flow with different wall temperature

The micro-Couette flow with different wall temperature is another test case for the present lattice Boltzmann model with the new slip boundary conditions. We could also find the effect of the Pr and Ec numbers on the velocity slips and temperature jumps with the same Knudsen number. From Fig. 5, it is found that the temperature profile becomes parabolic, when Ec is increased with fixed Kn and Pr number. On the other hand, as shown in Fig. 6, with the fixed Kn and Ec numbers, the effect of the viscous dissipation becomes notable when Pr is increased. The wall temperature jump increases with increasing Kn. When Ec increases to 1.0, as shown in Figs. 7 and 8, we find that the temperatures of the top wall boundary are very close to 1.01 with all different Kn numbers, which means that the temperature jump at the top wall boundary is almost zero, when Pr increased with $Ec=1.0$. When Ec exceed 1.0, as shown in Figs. 9-11, the comparison of temperature profile between the numerical simulation and analytic results is given at different Kn and Ec numbers. It is observed that the numerical results are in good agreement with the analytic ones. It is also found that the temperature at the upper boundary

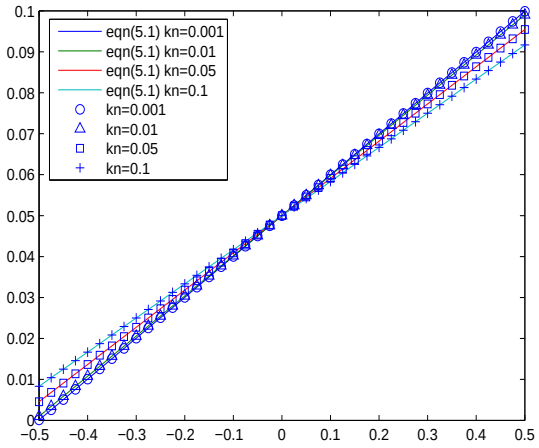

Figure 3: The velocity profile for $Kn=0.001$, 0.01, 0.05, 0.1, respectively.

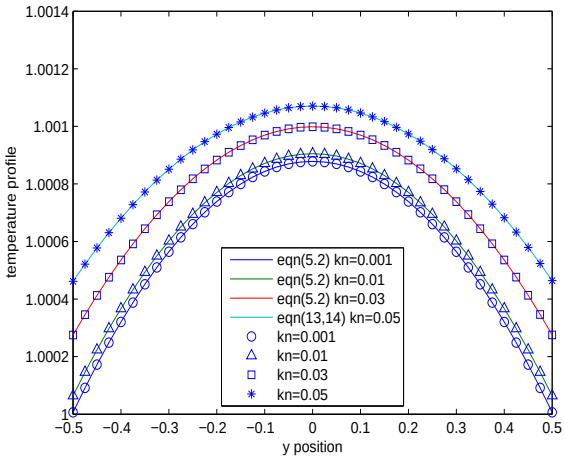

Figure 4: The temperature profile for $Kn=0.001$, 0.01, 0.03 and 0.05, respectively.

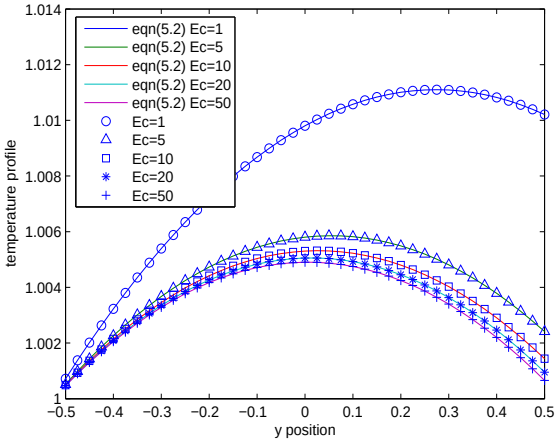

Figure 5: The temperature profile for $Ec=1$, 5, 10, 20, 50, respectively, with $Pr=5$, $Kn=0.1$.

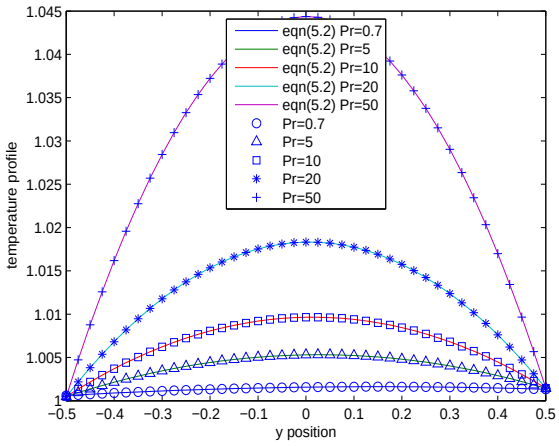

Figure 6: The temperature profile for $Pr=0.7$, 5, 10, 20, 50, respectively, with $Kn=0.1$, $Ec=10$.

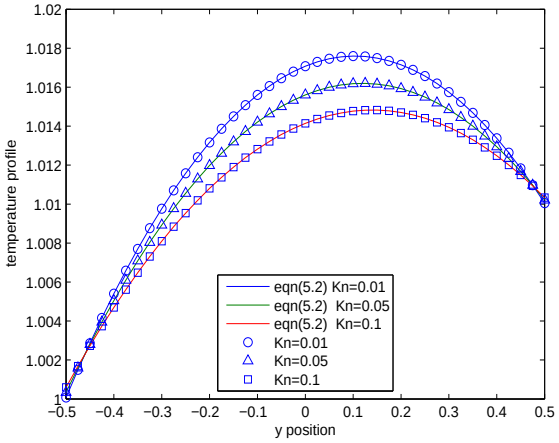

Figure 7: The temperature profile for $Kn=0.01$, 0.05, 0.1, respectively, with $Pr=10$, $Ec=1$.

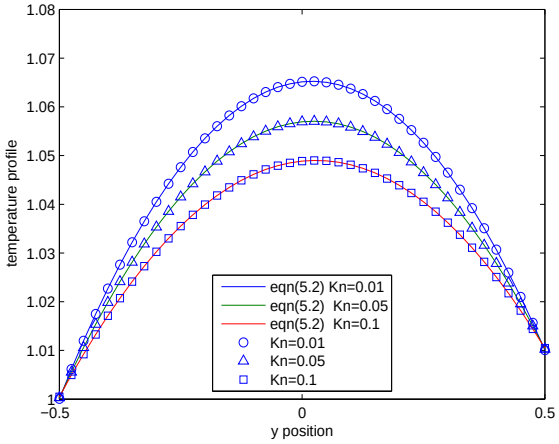

Figure 8: Same as Fig. 7, except with $Pr=50$, $Ec=1$.

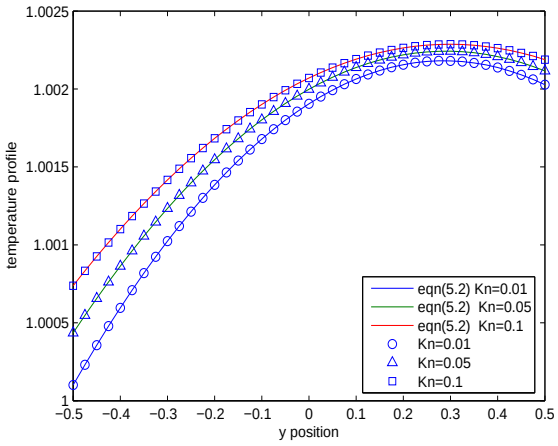

Figure 9: The temperature profile for $Kn=0.01$, 0.05, 0.1, respectively, with $Pr=0.7$, $Ec=5$.

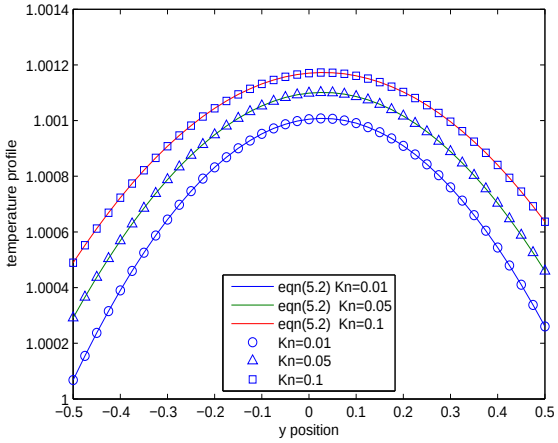

Figure 10: Same as Fig. 9, except with $Pr=0.7$, $Ec=50$.

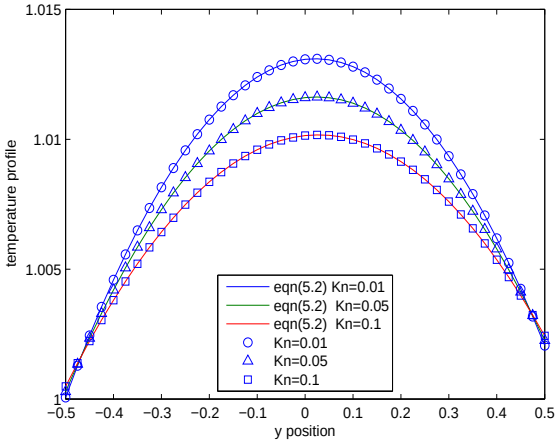

Figure 11: Same as Fig. 9, except with $Pr=10$, $Ec=5$.

is higher than that of the top wall and the temperature jump on the top boundary is negative with different Kn and Ec numbers.

7 Conclusion

The new slip boundary conditions for the TLBM were proposed in the present study. With two simple cases, we observed that the simulated velocity and temperature profiles are in good agreement with the analytic solutions. The slip length and the temperature jump agree well with the results of the DSMC, MD methods, which indicates the applicability of the present model and the new boundary treatment to describe the thermal microflow with viscous heat dissipation.

The TLBM with the new slip boundary conditions were applied to two problems: the thermal micro-Couette flow with a constant wall temperature and the thermal micro-Couette flow with different wall temperatures. For both problems, the velocity slips and temperature jumps at the walls become noticeable when the Knudsen number exceeds the value 0.01. Meanwhile, we find that the present model with the new slip boundary condition has good stability even as Pr and Ec numbers increased to 50.

Acknowledgments

The authors would like to thank Prof. Z. L. Guo and V. Sofonea for useful discussions. This study was financially supported by the National Basic Research Program of China (2006CB705804) and the National Natural Science Foundation of China (70271069).

References

[1] X. F. Peng, G. P. Peterson, B. X. Wang, Exp. Heat Transfer 7 (1994) 265.
[2] C. Yang, D. Li, J. H. Masliyah, Int. J. Heat Mass Tran. 41 (1998) 4229.
[3] G. E. Karniadakis, A. Beskok, Micro Flows: Fundamentals and Simulation, Springer-Verlag, New York, 2002.
[4] S. K. Loyalka, S. A. Hamoodi, Phys. Fluids A 2 (1990) 2061.
[5] T. Ohwada, Y. Sone, K. Aoki, Phys. Fluids A 1 (1989) 2042.
[6] B. J. Alder, T. E. Wainwright, J. Chem. Phys. 27 (1957) 1208.
[7] G. Bird, Molecular Gas Dynamics and the Direct Simulation of Gas Flows, Oxford Science Publications, 1994.
[8] X. B. Nie, G. D.Doolen, S. Y. Chen, J. Stat. Phys. 107 (2002) 279.
[9] S. Succi, Phys. Rev. Lett. 89 (2002) 064502.
[10] C. Y. Lim, C. Shu, X. D. Niu, Y. T. Chew, Phys. Fluids 14 (2002) 2299.
[11] Y. H. Zhang, R. S. Qin, D. R. Emerson, Phys. Rev. E 71 (2005) 047702.
[12] T. Lee, C. L. Lin, Phys. Rev. E 71 (2005) 046706.
[13] V. Sofonea, R. F. Sekerka, J. Compu. Phys. 207 (2005) 639.
[14] V. Sofonea, R. F. Sekerka, Phys. Rev. E 71 (2005) 066709.
[15] C. Shu, X. D. Niu, Y. T. Chew, J. Stat. Phys. 121 (2005) 239.

[16] Z. W. Tian, C. Zou, Z. H. Liu, Z. L. Guo, H. J. Liu, C. G. Zheng, Int. J. Mod. Phys. C 17 (2006) 603.
[17] Z. L. Guo, C. G. Zheng, B. C. Shi, Chinese Phys. 11 (2002) 366.
[18] Z. L. Guo, B. C. Shi, C. G. Zheng, Int. J. Numer. Fluids 39 (2002) 325.
[19] P. L. Bhatnagar, E. P. Gross, M. Krook, Phys. Rev. 94 (1954) 511.
[20] A. D'Orazio, S. Succi, C. Arrighetti, Phys. Fluids 15 (2003) 2778.
[21] L. B. Thomas, R. G. Lord, Comparative measurements of tangential momentum and thermal accommodations on polished and on roughened steel spheres, in: K. Karamcheti (Ed.), Rarefied Gas Dynamics, Academic Press, New York, vol. 8, 1974, pp. 405-412.
[22] A. Beskok, G. E. Karniadakis, J. Thermophys. Heat Tr. 8 (1994) 647.
[23] A. Beskok, Simulations and models for gas flows in microgeometrics, PhD Thesis, Princeton University, NJ, 1996.
[24] J. Dai, D. Xu, B. C. Khoo, K. Y. Lam, J. Micromech. Microeng. 10 (2000) 372.
[25] D. R. Willis, Phys. Fluids 5 (1962) 127.
[26] D. L. Morris, L. Hannon, A. L. Garcia, Phys. Rev. A 46 (1992) 5279.
[27] Y. Sone, T. Ohwada, K. Aoki, Phys. Fluids A 1 (1989) 363.
[28] Z. L. Guo, T. S. Zhao, Y. Shi, J. Appl. Phys. 99 (2006) 074903.